

Integrating Biocatalysts into Metal-Organic Frameworks: Disentangling the Roles of Affinity, Molecular Weight, and Size

Raphael Greifenstein,^[a] Dhana Röhrs,^[a] Tim Ballweg,^[a] Juliana Pfeifer,^[a] Eric Gottwald,^[a] Masanari Takamiya,^[b] Matthias Franzreb,^{*,[a]} and Christof Wöll^{*,[a]}

The integration of biocatalysts within metal-organic frameworks (MOFs) is attracting growing interest due to its potential to both enhance biocatalyst stability and sustain biocatalyst activity in organic solvents. However, the factors that facilitate the post-synthetic infiltration of such large molecules into MOF pores remain unclear. This systematic study enabled the identification of the influence of biocatalyst molecular size, molecular weight and affinity on the uptake by an archetypal MOF, NU-1000. We analyzed a range of six biocatalysts with

molecular weights from 1.9 kDa to 44.4 kDa, respectively. By employing a combination of fluorescence tagging and 3D-STED confocal laser scanning microscopy, we distinguished between biocatalysts that were internalized within the MOF pores and those sterically excluded. The catalytic functions of the biocatalysts hosted within the MOF were investigated and found to show strong variations relative to the solvated case, ranging from a two-fold increase to a strong decrease.

Introduction

Metal-organic frameworks (MOFs), synthesized through the coordination of di- or higher-topic organic ligands with metal ions or clusters, represent a highly versatile class of materials. Although initially developed for gas storage and separation,^[1–4] in recent years more advanced applications have emerged, including immobilizing and storing functional proteins.^[5–7] Owing to the extensive variety of available organic linkers and metal nodes accessible, metal-organic frameworks (MOFs) can be engineered with customizable geometries, enabling a huge variety of topologies. This versatility extends to the precise tuning of pore sizes and the dimensions of the pore entrances.^[8,9] The expansive surface area of metal-organic frameworks (MOFs) facilitates a substantial loading capacity for incorporated molecules. Simultaneously, the structural integrity of the framework offers protective support for delicate mole-

cules, like biocatalysts, shielding them from denaturation.^[10,11] As a result, for MOF-protected biocatalysts, also operation in organic solvents becomes possible.^[12] In general, MOF-based biocatalyst biocomposites can be classified according to their immobilization method; (i) encapsulation,^[13–16] (ii) post-synthetic infiltration,^[17–20] and (iii) adsorption on the outer surfaces of MOF particles.^[21–24] Every method of immobilization comes with its unique benefits. Notably, the process of encapsulation does not depend on the biocatalyst's size. The same applies for surface adsorption, where even the size of the pores and windows of the MOF framework do not play a crucial role – only the outer surface of the MOF particles is important. Conversely, when introducing the biocatalyst into the MOF post-synthetically, it is generally necessary for the pores of the MOF to be larger than the protein itself.^[25–27]

Notwithstanding this rule, there also exist reports claiming post-synthetic infiltration of proteins having sizes exceeding the diameter of the pores of the MOF. The explanatory hypothesis is a mechanism where the protein transiently unfolds to enable entry into the MOF and subsequently refolds upon gaining access to the pore interior.^[28] However, there is no clear experimental proof for this hypothesis and the thermodynamic driving force for an unfolding/refolding mechanism remains unclear. The situation could be different if unfolding is forced by organic solvents and refolding is triggered by switching back into an aqueous environment. Navarro-Sánchez et al. employed such a technique where they incubated protease, a crucial enzyme, in an organic solvent at moderate temperatures. This process apparently induced a partial unfolding of the enzyme, allowing it to pass through the pore windows of the MOF, despite these openings being only half the diameter of the enzyme when fully folded.^[20] Lian et al. analyzed the three different mesoporous cavities of MOF PCN-333 (small cavity 1.1 nm, medium cavity 3.4 nm with 2.6 nm window, large cavity

[a] R. Greifenstein, D. Röhrs, T. Ballweg, J. Pfeifer, E. Gottwald, M. Franzreb, C. Wöll
Institute of Functional Interfaces (IFG), Karlsruhe Institute of Technology (KIT), Bld. 330, Hermann-von-Helmholtz-Platz 1, Eggenstein-Leopoldshafen 76344, Germany
E-mail: christof.woell@kit.edu
matthias.franzreb@kit.edu

[b] M. Takamiya
Institute for Biological and Chemical Systems (IBCS), Karlsruhe Institute of Technology (KIT), Bld. 439, Hermann-von-Helmholtz-Platz 1, Eggenstein-Leopoldshafen 76344, Germany

Supporting information for this article is available on the WWW under <https://doi.org/10.1002/cbic.202400625>

© 2024 The Author(s). ChemBioChem published by Wiley-VCH GmbH. This is an open access article under the terms of the Creative Commons Attribution Non-Commercial License, which permits use, distribution and reproduction in any medium, provided the original work is properly cited and is not used for commercial purposes.

5.5 nm with 3.5 nm window^[29] after the infiltration of tyrosinase (TYR, 43 kDa, 5.5×5.5×5.6 nm). Only the 5.5 nm cavity was accommodated by TYR.^[30] A similar behavior was recorded by the same group with the MOF PCN-888 (small cavity 2 nm, medium cavity 5 nm with 2.5 nm window, large cavity 6.2 nm with 3.5 nm window) and the enzymes glucose oxidase (GOx, 160 kDa, 6.0×5.2×7.7 nm) and horseradish peroxidase (HRP, 44 kDa, 4.0×4.4×6.8 nm). GOx did only enter the large cavity and HRP the large and the medium. By encapsulation both enzymes with a specific order (GOx first, followed by HRP), they made use of this phenomenon and a tandem nanoreactor could be built. Besides to the retention by the small pore windows, π -stacking between the immobilized enzyme and the conjugated ligands of the MOF was suspected to prevent the enzyme from leaching. It was also assumed that the enzymes unfolded and refolded to fit through the pore windows, which have a cross-section smaller than the diameter of the enzymes.^[31]

Chen et al. suggested that the successful post-synthetic infiltration of microperoxidase-11 (MP-11, with a molecular weight of 1.9 kDa and dimensions of 1.1×1.7×3.3 nm) into the pores of Tb-mesoMOF can be attributed to the strong attraction between the biocatalyst and the MOF pores, likely due to the π -stacking interactions between the heme group in MP-11 and the triazine and benzene rings present in the organic ligands of Tb-mesoMOF. They also observed that the rate of MP-11 leakage from the MOF structure was notably slow. Therefore, they proposed that π -stacking interactions act as a barrier to prevent MP-11 from escaping the Tb-mesoMOF framework.^[32] Another effect for holding biocatalysts in MOF pores was presented by Yang et al. when investigating the embedding of lipase (3.0×4.0×5.0 nm) into the MOF PCN-333. They proposed that in this case the van der Waals forces between the alumina-clusters in PCN-333 and the amino ($-\text{NH}_2$) groups of biocatalysts play a significant role.^[33]

Given the diverse range of proposed mechanisms and constraints for the introduction of biocatalysts into MOF pores, we thoroughly examined the effect of MOF pore size on protein absorption. We used MOF NU-1000 in conjunction with six different-sized biocatalysts for our analysis. NU-1000 features an array of one-dimensional channels with a diameter of 3.1 nm, eliminating the need to consider smaller connecting windows between MOF pores (as discussed above). Of course, one still has to consider surface barriers, which might limit the uptake of molecules into these porous materials.^[34] We utilized various analytical techniques in a complementary fashion to distinguish between actual infiltration into the MOF and superficial adsorption on the exterior of MOF particles. Our research allows to derive a clear depiction of the assortment of factors that determine how biocatalysts are taken up by MOF pores.

Experimental Section

Materials and Reagents

All reagents and solvents used were of commercially available grade and used without any additional purification. NU-1000 was

purchased from cd-bioparticles, UK. The quality of the MOF particles (3 μm average length and 0.5 μm average diameter) was controlled by XRD. Tris(hydroxymethyl)aminomethane (Tris), sodium chloride, tri-sodium citrate dihydrate, 4-nitrophenyl acetate (pNPA), CytC, MP-11 and HRP were purchased from Merck, Germany and used as received. Bradford Reagent and 2,2'-azino-bis(3-ethylbenzthiazoline-6-sulfonic acid) (ABTS) were supplied by Thermo Fisher Scientific, Karlsruhe, Germany. Lysozyme was purchased from Carl Roth, Germany. The esterase AaEST2-His (EC 3.1.1.1) was prepared as described before.^[35] UPO was provided by the group of Frank Hollmann (Department of Biotechnology, University of Technology, NL).

Infiltration of Biocatalysts into NU-1000

For immobilization into the NU-1000 MOF powder material, the biocatalyst stock solutions were diluted to 30 $\mu\text{g}/\text{mL}$ and 300 $\mu\text{g}/\text{mL}$ in a TBS (Tris-buffered saline) (150 mM Tris, 150 mM NaCl, pH 8). 1 mL of the biocatalyst solution was added to 1 mg NU-1000 powder and mixed by repetitive pipetting until a uniform suspension was obtained. The well-dispersed solids were then incubated for 22 h at room temperature in an overhead shaker. The resulting biocatalyst@MOF composites were then isolated by centrifugation at 12,100 $\times g$ for 2 min, and the supernatant was decanted and kept for analysis. The biocatalyst@MOF was washed two times with 0.5 mL TBS, and stored in 0.5 mL TBS. The supernatant of the washing steps was also kept for analysis. The amount of biocatalysts loaded into the NU-1000 powder was determined by subtracting the mass of biocatalysts measured in the supernatants from the infiltrated biocatalyst mass. The biocatalyst mass in the supernatants was measured by Bradford assay. 150 μL of sample was mixed with 150 μL of Bradford reagent and incubated for 10 min at room temperature. The protein content of the sample was measured at 595 nm using a Tecan spectrophotometer and calculated with a BSA calibration curve.

Esterase Activity Assay

The activity of either free esterase or esterase loaded into NU-1000 was measured with the hydrolysis of pNPA using a spectrophotometer. The absorbance data at 405 nm - pNP absorption - were collected versus time. Stock solutions of pNPA (50 mM) were prepared utilizing DMSO as a diluent, followed by their dilution to 600 μM in TBS. The concentrations of NU-1000-immobilized esterase suspension, as well as free esterase solution, were adjusted to produce an analogous increase in pNP adsorption over the same time period. The reactions were performed in a 96 well plate comprising 160 μL of TBS and 20 μL of esterase solution/esterase@NU-1000 suspension and reactions were started by adding 20 μL of 600 μM pNPA.

Oxidase Activity Assay

The activity of the oxidases MP-11, CytC, HRP and UPO, either free or loaded into NU-1000, was measured with the oxidation of ABTS. The absorbance data at 420 nm - oxidized ABTS - were collected versus time. Stock solutions of ABTS (3 mM) and H_2O_2 (40 mM) were prepared in 100 mM citrate buffer pH 4.4 (CB). Again, the concentrations of NU-1000-immobilized oxidase suspensions, as well as free oxidase solutions, were adjusted to produce an analogous increase in oxidized ABTS adsorption over the same time period. The reactions were performed in a 96 well plate comprising 150 μL of CB, 20 μL 3 mM ABTS and 10 μL 40 mM H_2O_2 and reactions were started by adding 20 μL of oxidase solution/oxidase@NU-1000 suspension.

Labeling Biocatalysts with Fluorescent Dye

To aid in acquiring data on the spatial distribution, the biocatalysts were tagged with Cy5 NHS-ester at a molar ratio of 1.8:1. The biocatalyst solutions (250 μM) were prepared in a 1 M sodium bicarbonate buffer (pH 8.75). A Cy5 stock solution (8.1 mM) was prepared by dissolving Cy5 NHS-ester in DMSO. The biocatalyst and Cy5 stock solutions were diluted accordingly with 1 M sodium bicarbonate buffer and mixed to a solution of 130 μL , with 100 μL of biocatalyst and 30 μL of Cy5 solution. After 1 h of incubation the labeled biocatalysts were purified by size-exclusion chromatography in centrifuge columns with a buffer exchange to TBS, except for MP-11. Cy5-labeled MP-11 was purified by dialysis using the Dialysis Kit Pur-A-Lyzer Midi 1000 by Merck, with buffer exchange to TBS.

Confocal Laser Scanning Microscopy

The loading capacity of NU-1000 with fluorescent dye labeled biocatalysts was investigated using confocal laser scanning microscopy (CLSM) with a Leica Stellaris 5 instrument. Laser settings: WLL (white light laser) was used with the output power set to 85%. The 485 nm laser line power was adjusted to 9.99% and the 633 nm laser line was adjusted to 7.63%. The smart gain for the 485 nm channel 500–569 nm was set to 170.1%, the smart gain for the 633 nm channel 643–717 nm was set to 143.9% and the bright field channel to 26.1%. Laser scan speed was set to 400 Hz, Line Average was set to 32 using the 63x oil immersion objective. The images were digitally zoomed by a factor of 5.

Confocal 3D-STED Laser Scanning Microscopy

As a proof of concept experiment for the loading of NU-1000 particles with Cy5-labeled EST2, we performed confocal 3D-STED laser scanning microscopy using a Leica TCS-SP8-STED3X microscope (Leica Microsystems, Wetzlar). The instrument is equipped with a white light laser that was used for excitation at 633 nm and set to 85% output power and 0.2% intensity. Cy5 fluorescence was detected by the HyD detector through a 646–702 nm window with the smart gain set to 100% at 400 Hz scan frequency and unidirectional scan mode. The pinhole size was set to 0.6 Airy unit (105 μm) calculated at 670 nm as the peak emission wavelength of Cy5. The STED laser line of 775 nm was used set to 47.3% output power and 67.3% intensity. The images were taken using a 100x oil immersion STEDWHITE objective (HC PL APO CS2 100x/1.40 OIL) with a line average set to 4 and a digital zoom of 40x with an intensity depth of 16 bit. The z-stacks of 512 \times 512 XY pixel arrays were recorded with a resulting pixel size of 5.687 nm in x- and y-

direction and a voxel size of 80.109 nm in z-direction. The raw data images were processed using Fiji 1.54f.

Results and Discussion

The structural design of the MOF NU-1000 is well-documented^[36] and features zirconia clusters connected by pyrene-based organic linkers, featuring a mesoporous, channel-type framework with hierarchical channeling. The larger, hexagonal channels have a diameter of 3.2 nm, (see Figure 1) while the smaller, triangular channels are 1.2 nm wide with 0.8 nm windows connecting the channels. The structure of NU-1000 combined with its high stability in aqueous solution make it an ideal carrier for biocatalysts.

The properties of the different biocatalysts microperoxidase-11 (MP-11), lysozyme (Lys), cytochrome c (CytC), esterase (Est2), horseradish peroxidase (HRP) and unspecific peroxidase (UPO) studied in this article are listed in Table 1. Each of the biocatalysts was incubated with the NU-1000 MOF particles for 22 h. The biocatalyst mass used for loading was first kept around 30 μg biocatalyst per mg MOF and afterwards 300 $\mu\text{g}/\text{mg}$.

Figure 2A shows the biocatalyst loading capacities resulting from a low initial biocatalyst mass concentration of 30 μg per mg of MOF. Despite the excess MOF, only approximately 30–35% of the small biocatalysts MP-11, CytC, and Lys infiltrate into the MOF, corresponding to approximately 10–12 $\mu\text{g}/\text{mg}$ loading capacity. Since these low loading capacities cannot be attributed to steric limitations imposed by the available pore volume, it appears that the biocatalysts MP-11, CytC, and Lys possess only moderate affinity for infiltration into the NU-1000 structure. A different scenario is observed for the biocatalyst Est2, which is practically entirely taken up by the NU-1000 crystals, resulting in loading capacities of 30 $\mu\text{g}/\text{mg}$. It is important to highlight that according to the data provided in Table 1, Est2 is oversized by 15% for direct insertion into the one-dimensional channels of NU-1000. Therefore, slight conformational changes are necessary for Est2 to decrease its diameter. As previously observed in a separate study, the MOF NU-1000 appears to exhibit an unusually high affinity for

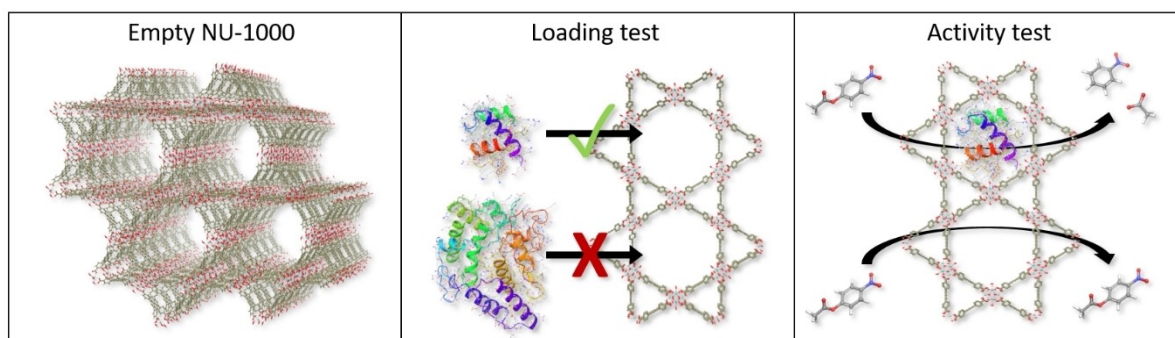
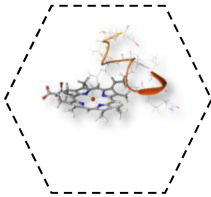
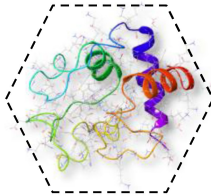
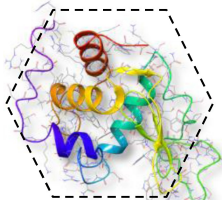

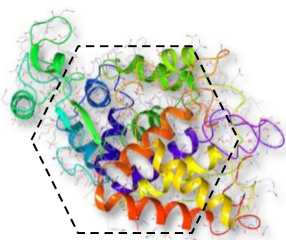
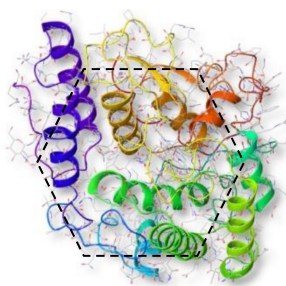


Figure 1. Schematic illustration of NU-1000's pore structure and of the conducted infiltration and activity tests. (A) Crystal structure of NU-1000 forming one-dimensional channels of almost cylindrical shape, (B) Post synthesis loading tests in aqueous testing the infiltration of six different biocatalysts, (C) Activity tests of the loaded biocatalysts applying small biocatalyst specific educts.

Table 1. Masses and dimensions of the biocatalysts investigated. The dashed line illustrates the cross-section of a NU-100 channel.

Biocatalyst	Mass (kDa)	Dimension (nm)	Scheme	Reference
MP-11	1.9	1.1×1.7×3.3		(Feng et al. 2015)
CytC	12.4	2.6×3.2×3.3		(Feng et al. 2015)
Lys	14.4	2.8×3.3×4.6		(Weiss, Palm, and Hilgenfeld 2000)
Est2	35	3.7×4.4×5.4		(De Simone et al. 2000)
HRP	44	4.0×4.4×6.8		(Feng et al. 2015)
UPO	44.4	3.9×5.0×5.5		(Ramirez-Escudero et al. 2018)

absorbing Est2. Despite the anticipated strong attraction to the components of NU-1000, the bigger biocatalysts HRP and UPO demonstrate the least amount of biocatalyst infiltration. This is expected because the cross-sectional area of these proteins is

significantly greater than the one-dimensional channel diameters of NU-1000. To estimate the dimensionless distribution coefficients, the loading capacities resulting from an initial biocatalyst mass concentration in solution of 30 μg per mg of

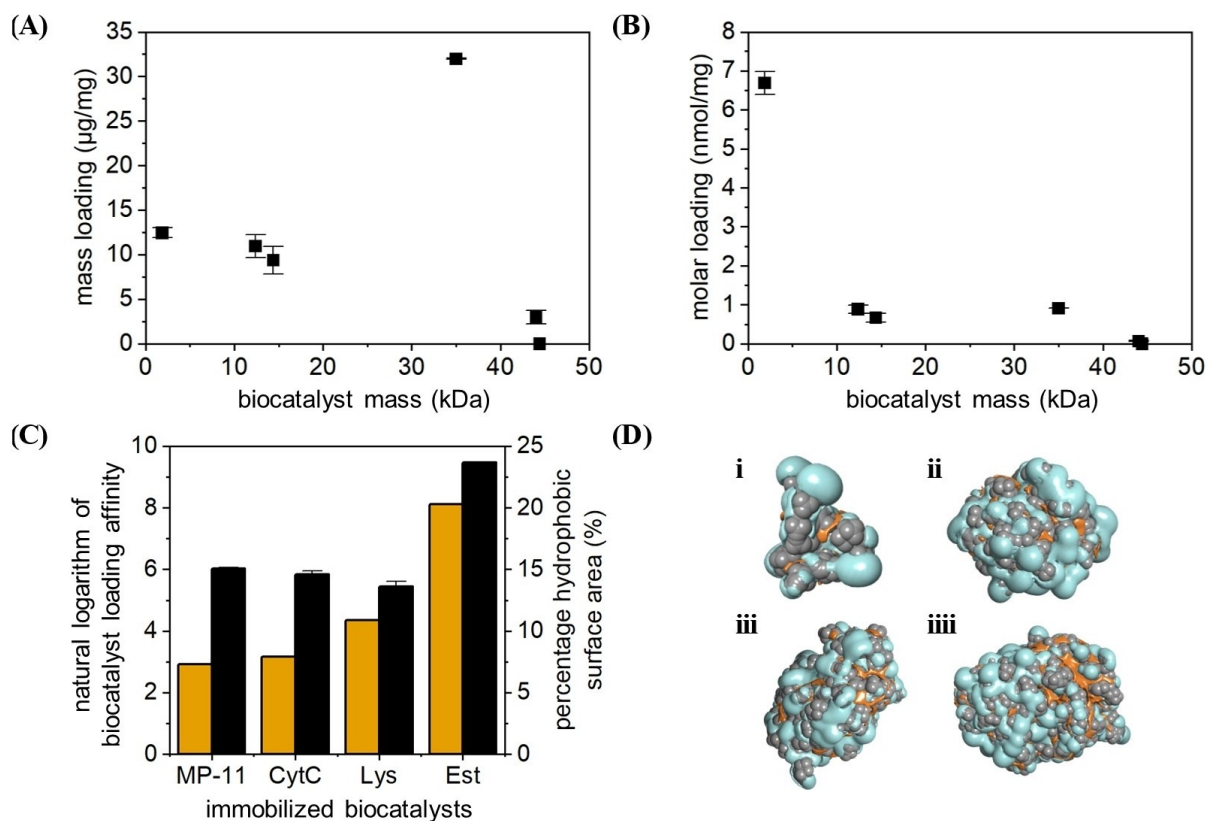


Figure 2. Biocatalyst loading capacities in NU-1000 as (A) mass loading and (B) molar loading in dependence of the molecular masses of the biocatalysts, (C) comparison of the natural logarithm of the dimensionless distribution coefficients (black) and the percentage of the hydrophobic surface area (orange) of the investigated biocatalysts, and (D) an illustration of hydrophobic (orange) and hydrophilic (blue) patches on the biocatalyst surface of MP-11 (i), CytC (ii), Lys (iii) and Est2 (iiii), calculated by the simulation software Schrödinger. The maximum achievable loading capacities were about 30 µg biocatalyst per mg MOF.

MOF were additionally plotted as molar loadings in Figure 2B. The dimensionless distribution coefficient is defined as the ratio between the protein concentration within the MOF and within the surrounding bulk fluid (supernatant) after equilibration at the end of the loading experiments. For calculating the ratio, both concentrations must be expressed in the same terms. In our case we used nmol/ml. The concentrations within the supernatant and within the MOF are listed in Table S1 of the supporting information. Assuming absorption behavior still within the linear range, dimensionless distribution coefficients of 412, 343, 230 and 13023 can be estimated for MP-11, CytC, Lys, and Est2. In analogy to the thermodynamic relationship between the change in free energy during a reaction and the natural logarithm of its equilibrium constant it can be shown that the correlation also holds between the free energy change during an adsorption process and the corresponding distribution coefficient.^[41] Therefore, despite the simplifying assumptions, the distribution coefficient demonstrates the significantly higher affinity of NU-1000 towards Est2 compared to MP-11, CytC and Lys. Unfortunately, due to steric exclusion, it is not possible to calculate a thermodynamically determined distribution coefficient for the larger biocatalysts HRP and UPO. Interestingly, the calculated distribution coefficients for MP-11, CytC, Lys, and Est2 correlate qualitatively with the proportion of hydrophobic patches on the biocatalyst surface, calculated by

the simulation software Schrödinger (see Figure 1D and Table 2). While MP-11 exhibits the lowest hydrophobic surface fraction and CytC and Lys possess only 7.9% and 10.9% hydrophobic surface fractions, respectively, Est2 shows a fraction of over 20%. This finding supports the hypothesis proposed by Lykourinou et al. that hydrophobic interactions play an important role in the infiltration and stable binding of biocatalysts in MOFs.^[40]

Assuming that the free energy change is mainly caused by the interaction of the hydrophobic patches and the MOF pores we plotted the percentage of these patches besides the natural logarithm of the experimentally determined loading affinity constants (see Figure 1C). The plot shows a correlation between these quantities, whose accuracy is of course limited by the fact that only hydrophobic interactions were considered. For a more precise estimation of the loading affinity constants, numerous other potential interactions would have to be taken into

Table 2. Hydrophobicity of the biocatalyst surface areas.						
Biocatalyst	MP-11	CytC	Lys	Est2	HRP	UPO
Percentage hydrophobic surface area (%)	7.3	7.9	10.9	20.3	20	19.7

account, such as hydrogen bonds, electrostatic forces, and π -stacking.

In a second series of experiments, the same amount of MOF particles was contacted with ten times the biocatalyst quantity, i.e., 300 μg per mg of MOF. The rationale behind this approach was that a sufficiently high biocatalyst concentration would be enough to saturate the MOF loading. The resulting loading capacities are shown in Figures 3A and B. The results exhibit a clear trend, with the exception of lysozyme. When biocatalysts are sterically capable of infiltrating the MOF pores, higher molecular weights correlate with higher saturation loadings. However, this correlation is not linear; instead, it demonstrates an approximate proportionality to the square root of the molecular weight. Conversely, the nonlinearity of the correlation between saturation loading and molecular weight implies that the achievable molar saturation loading of biocatalysts decreases with increasing molecular weight. As explained in the supporting information, a linear dependence between saturation loading and the cube root of the molecular weight squared is consistent with the assumption that biocatalysts line up one after another in the channels without overlapping. This hypothesis agrees well with the experimental data as seen in Figure 3C. This leads to an increasing portion of unused pore volume for smaller biocatalysts, as depicted in the schemes in Figure 3D. Interestingly, the assumption of non-overlapping

even holds true for the smallest biocatalyst investigated, MP-11. However, a closer examination reveals that the intuition regarding the relationship between molecular weight ratios and resulting size ratios can be deceptive due to the molecular weight growing in the third power with molecular size. Table 1 shows that even for MP-11, the smallest biocatalyst investigated here, one of the perpendicular axes describing the ellipsoid circumscribing the molecule is larger than the diameter of the one-dimensional channels of NU-1000. The reason why the saturation loading for lysozyme deviates significantly from the assumed correlation is currently unclear. We speculate that strong interactions between the cysteine-rich structure of lysozyme and the MOF structure may hinder the effective transport of the biocatalyst into the pores. Looking at the absolute values of the achieved biocatalyst loading capacities it becomes obvious that these are lower than reported for comparable biocatalysts and the same MOF in literature but also in our own previous work.^[12,42] Nevertheless, all experiments shown in Figures 2 and 3 were conducted with the same batch of commercial NU-1000 particles, allowing the mutual comparison of the achieved loading capacities. The reduced absolute loading capacities may be caused by different synthesis conditions of the commercial batch.^[34,43]

To investigate whether the immobilization has an impact on the catalytic activity of the biocatalysts, the mass specific

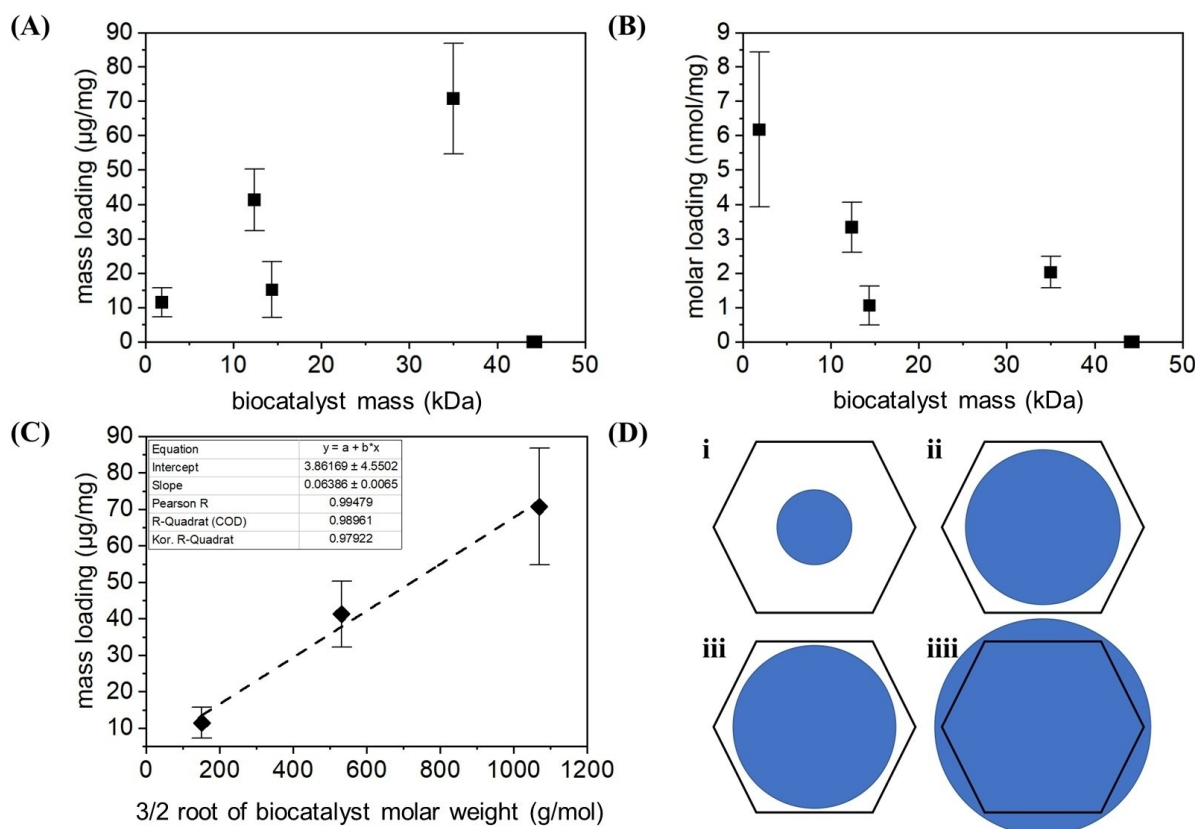


Figure 3. Biocatalyst loading capacities in NU-1000 as (A) mass loading and (B) molar loading in dependence of the biocatalyst masses, (C) mass loading of the biocatalysts MP-11, CytC and Est2 over the cube root of their molar weight squared and (D) an illustration of the size of the biocatalysts (blue circles representing the diameter of hypothetical spheres having the same volumes than the biocatalysts) MP-11 (i), CytC (ii), Lys (iii) and Est2 (iiii) compared to the NU-1000 channels. The maximum achievable loading capacities were about 300 μg biocatalyst per mg MOF.

activities of free and immobilized biocatalysts were measured. Afterwards, the activity yield was calculated as the percentage of the activity of the immobilized biocatalysts to the activity of the free biocatalysts.

As seen in Figure 4, immobilized CytC and Est2 display higher specific activity when the loading was low. Since the loadings of MP-11 were almost the same regardless of the biocatalyst concentration applied during loading, similar activities were expected. This was also confirmed within the scope of experimental accuracy, with an activity yield between 50–70% in both cases. Interestingly, CytC@MOF showed twice the specific activity of free CytC in case of a moderate loading capacity of 11 $\mu\text{g}/\text{mg}$. This unusual phenomena was already reported by the group of Farha,^[44] and explained by conformational changes of the active center of CytC caused by the immobilization.^[44] The loading of four times the amount of CytC resulted in the reduction of the specific activity yield by half. Substrate and product diffusion could be sterically hindered for CytC being immobilized deeper in the MOF channels. Est2 immobilized in the MOF channels have the smallest activity yield with 7.5% for low loading. As mentioned before, Est2 undergoes conformational changes to fit in the NU-1000 channel. This could lead to changes in the active center causing the reduction in activity. In addition, Est2 completely fills the channel and can't move, which may sterically hinder the accessibility of the active site to the substrate. By loading about two times more Est2, its specific activity is reduced even further. Since there was almost no loading for HRP and UPO, no activity could be measured, or the activity measured was due to biocatalysts adsorbed to the outer surface of the MOF. No activity assay was available for Lys at this time.

With the exception of CytC, the specific catalytic activity of all biocatalysts reduced after immobilization into the MOF particles. However, it is reported that this loss can be compensated by an increase in the stability, meaning the immobilized biocatalysts stay active for longer periods of time compared to their freely dissolved form stored under the same conditions. In order to test their long term stability, we

incubated immobilized samples of the biocatalysts which were able to infiltrate NU-1000 in TBS buffer at 6 °C up to 48 days. During this period the remaining activity was sporadically tested to monitor the gradual deactivation. While the procedure worked fine for EST2, the incubation of the immobilisates of smaller biocatalysts in plain TBS buffer over several days revealed that the binding affinity towards the MOF is not high enough and the biocatalysts slowly leached back into the solution. Therefore, measuring the long-term catalytic activity of the immobilized form of these biocatalysts was not possible. In contrast, EST2 at least partly stayed in the NU-1000 particles for 48 days and showed a reproducible half-life period of approx. 25 days, which is more than 10 times the half-life period of freely dissolved EST2 stored at the same conditions (Figure 4B).

To demonstrate, that the biocatalysts are immobilized inside of the NU-1000 channels, Cy5-labeled biocatalysts were incubated with NU-1000. The MOFs were analyzed by in situ confocal laser scanning microscopy (CLSM, Figure 5) directly after the start of the incubation (Figure 5A–F i), and after 22 h (Figure 5 A–F ii).

For all biocatalysts, the image at the start of the incubation shows a fluorescent adlayer on the outer surface of NU-1000 and at the ends of the MOF. The images after 22 h of incubation of Cy5-labeled Lys, CytC and Est2 (Figure 5 B–D ii) show a strong fluorescence at the ends of NU-1000 that gets weaker towards the center of the MOF. The observed spatial distribution of the fluorescence cannot be explained by multi-layer adsorption at the outer MOF-surface as we demonstrated by CLSM experiments with MOFs preloaded with unlabeled biocatalyst in our previous publication.^[12] On the other hand, after 22 h incubation of Cy5-labeled MP-11, HRP and UPO with NU-1000 (Figure 5 A, D, E ii), the images do not differ from those at the start of the incubation. This indicates, that all biocatalysts first adsorb at the outer surface of the MOF and afterwards diffuse into the NU-1000 channels, if they fit in, except MP-11. As seen in Table 2, MP-11 has the least percentage hydrophobic area, which could mean it has the

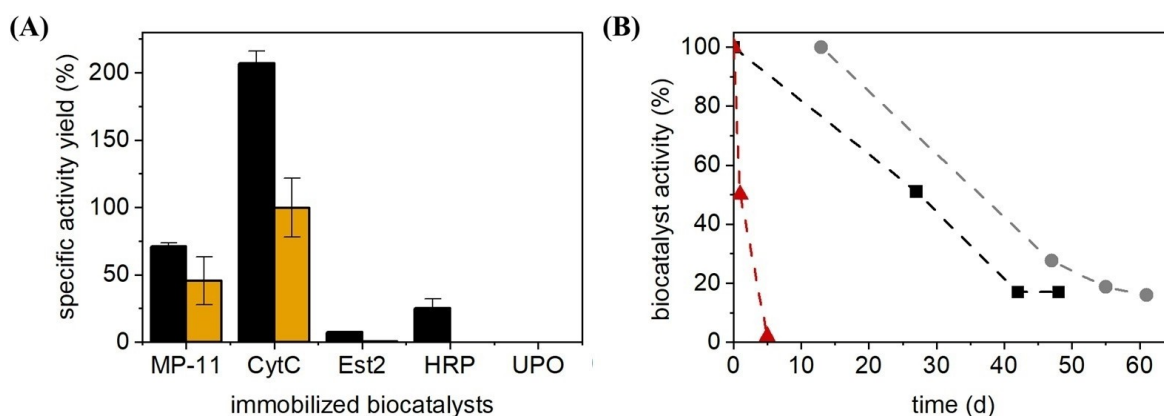


Figure 4. A: Mass specific activity yield of biocatalyst@MOF with low loading (black) and high loading (yellow). B: Test of the long-term stability of EST2@MOF and free EST2 in aqueous solution. EST2@MOF (black square and grey dot) and free EST2 (red triangle) were incubated in TBS (150 mM Tris, 150 mM NaCl, pH 7.4) for 48 days and 7 days respectively. The test series indicated by the grey dots was started with a two-week delay with a new batch of NU-1000 particles. The measured activities of the samples taken were calculated as residual activity based on the activity of the first sample.

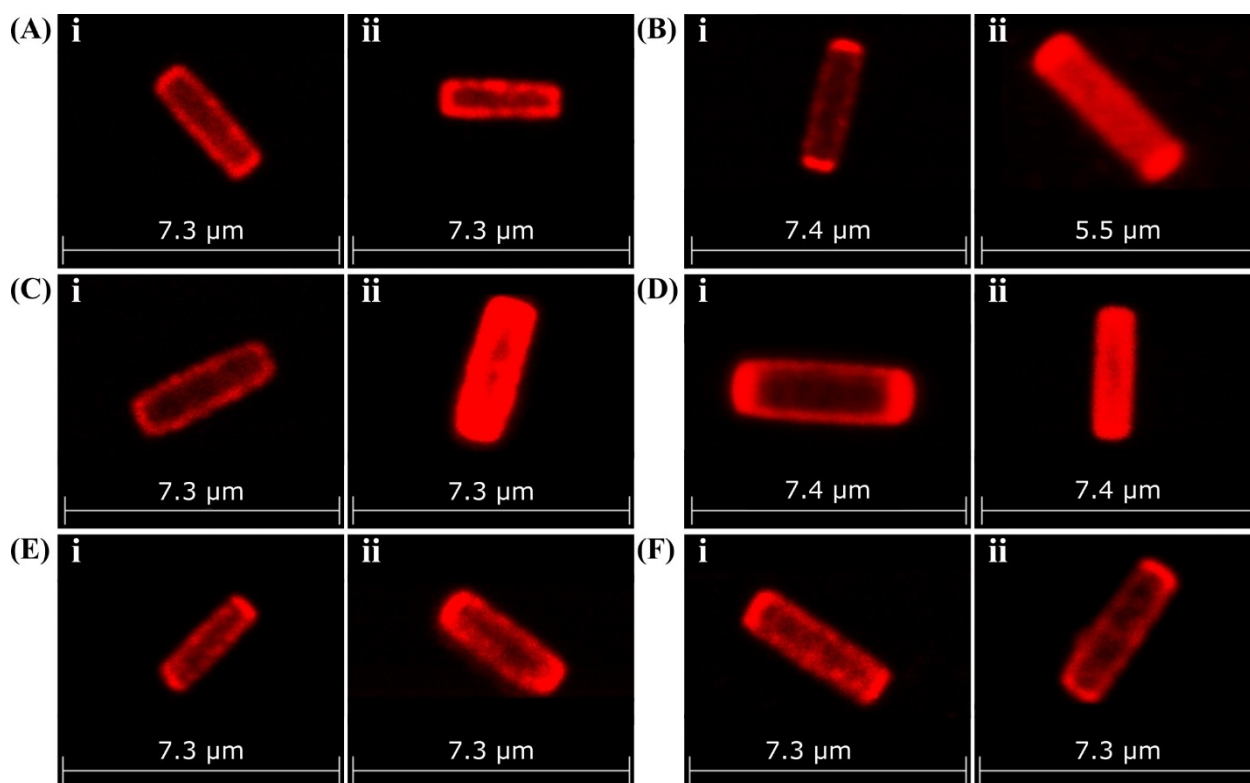


Figure 5. Confocal laser scanning microscopy (CLSM) of fluorescent dye labeled (A) MP-11, (B) CytC, (C) Lys, (D) Est2, (E) HRP, (F) UPO. The images were taken at the (i) start of the incubation and (ii) after 22 h.

least affinity to load into NU-1000. Also, since MP-11 is only three times the size of the fluorescent dye, the labeling may also have partially failed or the fluorescent tag influenced the immobilization process. Thereby unlabeled MP-11 could be preferably loaded in the MOF, and only a reduced fluorescence can be seen. For HRP and UPO, the absence of fluorescence at the center of the MOF supports the results from the loading experiments, demonstrating no loading of HRP and UPO into NU-1000.

While the CLSM images presented in Figure 5 allow an impression of the biocatalyst distribution along the xy-plane, the resolution in z-direction is limited to approx. 500 nm, which is the same than the diameter of the applied MOF crystals. Therefore, the images do not allow a real 3D representation and insightful cross-sectional cuts through the particle at different levels. In order to overcome this limitation, we conducted additional high-resolution 3D-STED microscopy for the case of NU-1000 particles infiltrated with Cy5-labeled esterase. Esterase was selected because it is the largest representative among the biocatalysts which showed to be able to enter the NU-1000 pores. The NU-1000 particles were loaded with Cy5-labeled esterase as described in the Materials & Methods section. After 22 h, the loading was analyzed by confocal 3D-STED microscopy. As can be seen from Figure 6, the incubation of the NU-1000 particle with Cy5-EST2 resulted in a homogeneous loading of the entire z-direction of the particle. Images 1 to 5 correspond to images no. 7 to 27 of the stack comprising 44 images in total. With the chosen settings,

the achieved resolution in z-orientation was 80 nm. An intensity scan across the same sections confirmed the impression that the loading resulted in a homogeneous distribution of Cy5-EST2 along the full depth of the particle (Figure 6, Bottom). In a control experiment we incubated NU-1000 particles with unlabeled EST2 for 22 h and afterwards incubated them with Cy5-labeled EST2. As obvious from Figure S1 in the supporting information, showing the slices and the corresponding orthogonal projections at the indicated positions, nearly no fluorescence could be detected inside the particles.

Conclusions

In this study, we explored how six distinct biocatalysts of varying sizes are immobilized in the Metal-Organic Framework (MOF) known as NU-1000. Our findings demonstrated that biocatalysts such as MP-11, CytC, Lys, and Est2 successfully penetrated into the channels of NU-1000. In contrast, HRP and UPO either adhered only to the external surfaces of the MOF particles or failed to integrate at all. This behavior aligns with a size exclusion principle, where biocatalysts exceeding the channel dimensions of NU-1000 are unable to access its interior. Notably, biocatalysts slightly larger than the channels could still infiltrate if the driving forces are sufficiently strong, like significant hydrophobicity on their exterior surfaces. This suggests that the tendency for proteins to infiltrate NU-1000 is influenced by hydrophobic interactions with the MOF's inner

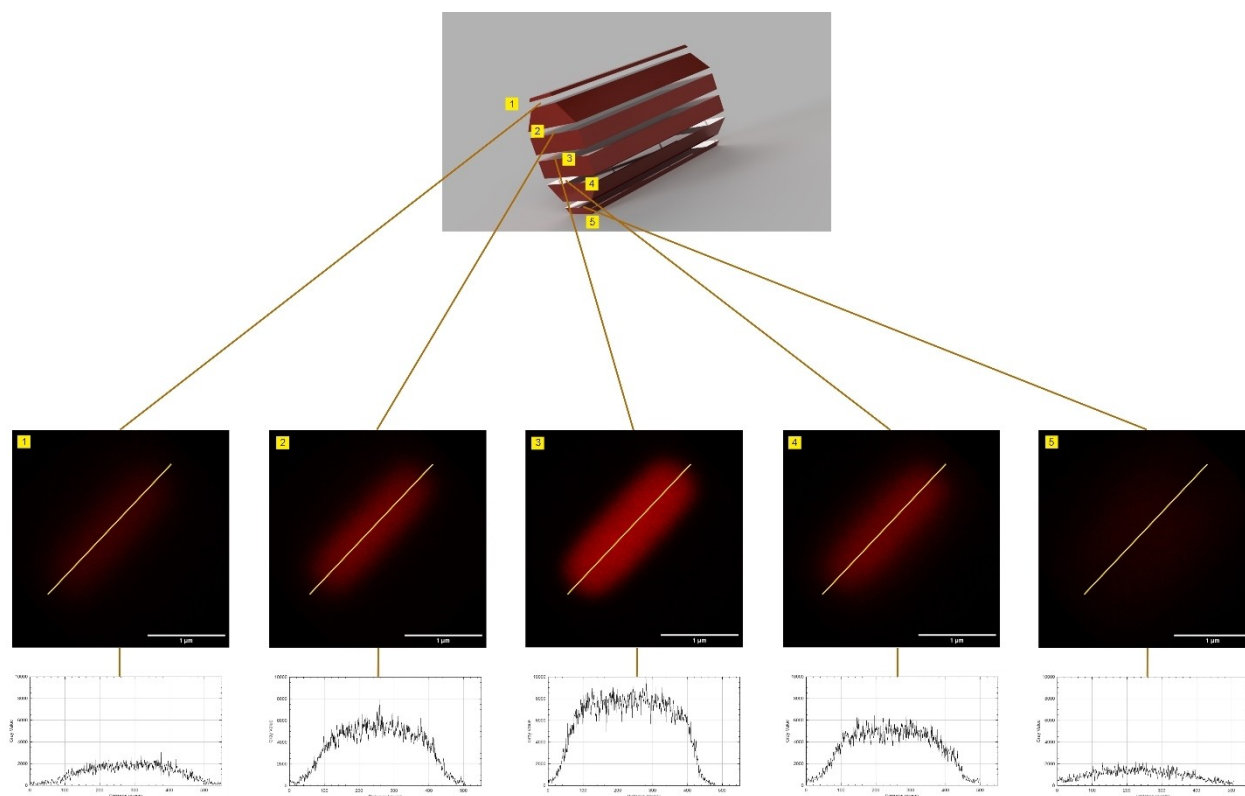


Figure 6. Top: Sketch of a NU-1000 particle with 2 μm length and 0.5 μm width being divided into five layers along the z-plane. Middle: 3D-STEP images of the five layers, imaged in z-direction with a step size of 80 nm. As can be seen, the NU-1000 particles are homogeneously loaded with Cy5-labeled EST2 along the xy-plane in each z-layer. Because the middle layer comprises a volume which is completely within the particle, it appears with the highest intensity. Layer above and below partly detect areas that are outside the particle and therefore show a reduced intensity. Bottom: This visual impression is confirmed by intensity scans across the marked yellow line in each z-layer.

surfaces. The importance of attractive interactions between the infiltrated biocatalysts and the hosting MOF was further confirmed by the long-term stability tests conducted. While Est2 showed a stable immobilization and strongly enhanced stability, smaller biocatalysts started leaching back into the solution when stored in plain buffer for several days. Although further experiments are needed in future, these results indicate that there not only exists an upper size limit for efficient immobilization of biocatalysts into MOFs, but also a lower size limit, because the size of the biomolecules needs to be sufficiently close to the pore size of the MOF to optimize binding affinity. As a consequence, the used MOF carrier should be optimized to achieve a close fit between the size of the biomolecule of choice and the MOF pores. An alternative is the use of modified ligands during MOF synthesis, which will allow the covalent binding of infiltrated small biomolecules, e.g. by NH_2 -groups.

Abbreviations

MOF metal-organic framework
MP-11 microperoxidase-11
Lys lysozyme
CytC cytochrome c

HRP horseradish peroxidase

UPO unspecific peroxidase

Author Contributions

The manuscript was written through contributions of all authors. All authors have given approval to the final version of the manuscript.

Acknowledgements

C.W. acknowledges support from the Deutsche Forschungsgemeinschaft (DFG, German Research Foundation) under the Germany Excellence Strategy via the Excellence Cluster 3D Matter Made to Order (grant no. EXC-2082/1-390761711). Additional financial support came from the Helmholtz program "Materials Systems Engineering" under the topic "Adaptive and Bioinspired Materials Systems" and the Joint Lab "Virtual Materials Design". Open Access funding enabled and organized by Projekt DEAL.

Conflict of Interests

The authors declare no conflict of interest.

Data Availability Statement

The data that support the findings of this study are available in the supplementary material of this article.

Keywords: Metal-organic frameworks · Biocatalyst immobilization · Enzyme activity

- [1] M. Kondo, T. Yoshitomi, H. Matsuzaka, S. Kitagawa, K. Seki, *Angew. Chem. Int. Ed. Engl.* **1997**, *36*, 1725–1727.
- [2] H. Li, M. Eddaoudi, T. L. Groy, O. M. Yaghi, *J. Am. Chem. Soc.* **1998**, *120*, 8571–8572.
- [3] K. Sumida, D. L. Rogow, J. A. Mason, T. M. McDonald, E. D. Bloch, Z. R. Herm, T.-H. Bae, J. R. Long, *Chem. Rev.* **2012**, *112*, 724–781.
- [4] J.-R. Li, J. Sculley, H.-C. Zhou, *Chem. Rev.* **2012**, *112*, 869–932.
- [5] S. Kitagawa, R. Kitaura, S. Noro, *Angew. Chem. Int. Ed.* **2004**, *43*, 2334–2375.
- [6] X. Lian, Y. Fang, E. Joseph, Q. Wang, J. Li, S. Banerjee, C. Lollar, X. Wang, H.-C. Zhou, *Chem. Soc. Rev.* **2017**, *46*, 3386–3401.
- [7] M. Ali, E. Pervaiz, T. Noor, O. Rabi, R. Zahra, M. Yang, *Int. J. Energy Res.* **2021**, *45*, 1190–1226.
- [8] J. Liu, J. Liang, J. Xue, K. Liang, *Small* **2021**, *17*, 2100300.
- [9] R. Haldar, A. Mazel, M. Krstić, Q. Zhang, M. Jakoby, I. A. Howard, B. S. Richards, N. Jung, D. Jacquemin, S. Diring, W. Wenzel, F. Odobel, C. Wöll, *Nat. Commun.* **2019**, *10*, 2048.
- [10] S. Huang, X. Kou, J. Shen, G. Chen, G. Ouyang, *Angew. Chem. Int. Ed.* **2020**, *59*, 8786–8798.
- [11] J. Liang, K. Liang, *Adv. Funct. Mater.* **2020**, *30*, 2001648.
- [12] R. Greifenstein, T. Ballweg, T. Hashem, E. Gottwald, D. Achauer, F. Kirschhöfer, M. Nusser, G. Brenner-Weiß, E. Sedghamiz, W. Wenzel, E. Mittmann, K. S. Rabe, C. M. Niemeyer, M. Franzreb, C. Wöll, *Angew. Chem. Int. Ed.* **2022**, *61*. DOI: 10.1002/anie.202117144.
- [13] K. Liang, R. Ricco, C. M. Doherty, M. J. Styles, S. Bell, N. Kirby, S. Mudie, D. Haylock, A. J. Hill, C. J. Doonan, P. Falcaro, *Nat. Commun.* **2015**, *6*, 7240.
- [14] R. C. Rodrigues, C. Ortiz, Á. Berenguer-Murcia, R. Torres, R. Fernández-Lafuente, *Chem. Soc. Rev.* **2013**, *42*, 6290–6307.
- [15] H. An, M. Li, J. Gao, Z. Zhang, S. Ma, Y. Chen, *Coord. Chem. Rev.* **2019**, *384*, 90–106.
- [16] W. Liang, P. Wied, F. Carraro, C. J. Sumbly, B. Nidetzky, C.-K. Tsung, P. Falcaro, C. J. Doonan, *Chem. Rev.* **2021**, *121*, 1077–1129.
- [17] C. Doonan, R. Riccò, K. Liang, D. Bradshaw, P. Falcaro, *Acc. Chem. Res.* **2017**, *50*, 1423–1432.
- [18] N. Ye, X. Kou, J. Shen, S. Huang, G. Chen, G. Ouyang, *ChemBioChem* **2020**, *21*, 2585–2590.
- [19] X. Wang, P. C. Lan, S. Ma, *ACS Cent. Sci.* **2020**, *6*, 1497–1506.
- [20] J. Navarro-Sánchez, N. Almora-Barrios, B. Lerma-Berlanga, J. J. Ruiz-Pernía, V. A. Lorenz-Fonfria, I. Tuñón, C. Martí-Gastaldo, *Chem. Sci.* **2019**, *10*, 4082–4088.
- [21] S. Jung, Y. Kim, S.-J. Kim, T.-H. Kwon, S. Huh, S. Park, *Chem. Commun.* **2011**, *47*, 2904–2906.
- [22] J. Mehta, N. Bhardwaj, S. K. Bhardwaj, K.-H. Kim, A. Deep, *Coord. Chem. Rev.* **2016**, *322*, 30–40.
- [23] T. J. Pisklak, M. Macías, D. H. Coutinho, R. S. Huang, K. J. Balkus, *Top. Catal.* **2006**, *38*, 269–278.
- [24] E. Gkaniatsou, C. Sicard, R. Ricoux, J.-P. Mahy, N. Steunou, C. Serre, *Mater. Horiz.* **2017**, *4*, 55–63.
- [25] E. Gkaniatsou, C. Sicard, R. Ricoux, L. Benahmed, F. Bourdreux, Q. Zhang, C. Serre, J. Mahy, N. Steunou, *Angew. Chem. Int. Ed.* **2018**, *57*, 16141–16146.
- [26] P. Li, S.-Y. Moon, M. A. Guelta, S. P. Harvey, J. T. Hupp, O. K. Farha, *J. Am. Chem. Soc.* **2016**, *138*, 8052–8055.
- [27] A. R. M. Silva, J. Y. N. H. Alexandre, J. E. S. Souza, J. G. L. Neto, P. G. de Sousa Júnior, M. V. P. Rocha, J. C. S. dos Santos, *Molecules* **2022**, *27*, 4529.
- [28] Y. Chen, V. Lykourinou, C. Vetromile, T. Hoang, L.-J. Ming, R. W. Larsen, S. Ma, *J. Am. Chem. Soc.* **2012**, *134*, 13188–13191.
- [29] D. Feng, T.-F. Liu, J. Su, M. Bosch, Z. Wei, W. Wan, D. Yuan, Y.-P. Chen, X. Wang, K. Wang, X. Lian, Z.-Y. Gu, J. Park, X. Zou, H.-C. Zhou, *Nat. Commun.* **2015**, *6*, 5979.
- [30] X. Lian, Y. Huang, Y. Zhu, Y. Fang, R. Zhao, E. Joseph, J. Li, J.-P. Pellois, H.-C. Zhou, *Angew. Chem. Int. Ed.* **2018**, *57*, 5725–5730.
- [31] X. Lian, Y.-P. Chen, T.-F. Liu, H.-C. Zhou, *Chem. Sci.* **2016**, *7*, 6969–6973.
- [32] Y. Chen, S. Han, X. Li, Z. Zhang, S. Ma, *Inorg. Chem.* **2014**, *53*, 10006–10008.
- [33] W. Yang, W. Liang, L. A. O'Dell, H. D. Toop, N. Maddigan, X. Zhang, A. Kochubei, C. J. Doonan, Y. Jiang, J. Huang, *JACS Au* **2021**, *1*, 2172–2181.
- [34] L. Heinke, Z. Gu, C. Wöll, *Nat. Commun.* **2014**, *5*, 4562.
- [35] R. Greifenstein, T. Ballweg, T. Hashem, E. Gottwald, D. Achauer, F. Kirschhöfer, M. Nusser, G. Brenner-Weiß, E. Sedghamiz, W. Wenzel, E. Mittmann, K. S. Rabe, C. M. Niemeyer, M. Franzreb, C. Wöll, *Angew. Chem. Int. Ed.* **2022**, *61*. DOI: 10.1002/anie.202117144.
- [36] T. Islamoglu, K. Otake, P. Li, C. T. Buru, A. W. Peters, I. Akpınar, S. J. Garibay, O. K. Farha, *CrystEngComm* **2018**, *20*, 5913–5918.
- [37] M. S. Weiss, G. J. Palm, R. Hilgenfeld, *Acta Crystallogr. D Biol. Crystallogr.* **2000**, *56*, 952–958.
- [38] G. De Simone, S. Galdiero, G. Manco, D. Lang, M. Rossi, C. Pedone, *J. Mol. Biol.* **2000**, *303*, 761–771.
- [39] M. Ramirez-Escudero, P. Molina-Espeja, P. Gomez de Santos, M. Hoffrichter, J. Sanz-Aparicio, M. Alcalde, *ACS Chem. Biol.* **2018**, *13*, 3259–3268.
- [40] V. Lykourinou, Y. Chen, X.-S. Wang, L. Meng, T. Hoang, L.-J. Ming, R. L. Musselman, S. Ma, *J. Am. Chem. Soc.* **2011**, *133*, 10382–10385.
- [41] Y. Liu, *J. Chem. Eng. Data* **2009**, *54*, 1981–1985.
- [42] P. Li, J. A. Modica, A. J. Howarth, E. Vargas, L. P. Z. Moghadam, R. Q. Snurr, M. Mrksich, J. T. Hupp, O. K. Farha, *Chem* **2016**, *1*, 154–169.
- [43] L. Heinke, C. Wöll, *Adv. Mater.* **2019**, *31*. DOI: 10.1002/adma.201806324.
- [44] Y. Chen, F. Jiménez-Ángeles, B. Qiao, M. D. Krzyaniak, F. Sha, S. Kato, X. Gong, C. T. Buru, Z. Chen, X. Zhang, N. C. Gianneschi, M. R. Wasielewski, M. Olvera de la Cruz, O. K. Farha, *J. Am. Chem. Soc.* **2020**, *142*, 18576–18582.

Manuscript received: July 27, 2024

Revised manuscript received: August 16, 2024

Accepted manuscript online: August 21, 2024

Version of record online: October 24, 2024